Mon. Not. R. Astron. Soc. **000**, 000–000 (0000) Printed 31 October 2018 (MN LATEX style file v2.2)

A powerful new method for probing the atmospheres of transiting exoplanets

I.A.G. Snellen ⋆
Institute for Astronomy, University of Edinburgh, Blackford Hill , Edinburgh EH9 3HJ, UK

Accepted .... Received ...; in original form ....

ABSTRACT

Although atmospheric transmission spectroscopy of HD209458b with the Hubble Space Telescope has been very successful, attempts to detect its atmospheric absorption features using ground-based telescopes have so far been fruitless. Here we present a new method for probing the atmospheres of transiting exoplanets which may be more suitable for ground-based observations, making use of the Rossiter effect. During a transit, an exoplanet sequentially blocks off light from the approaching and receding parts of the rotating star, causing an artificial radial velocity wobble. The amplitude of this signal is directly proportional to the effective size of the transiting object, and the wavelength dependence of this effect can reveal atmospheric absorption features, in a similar way as with transmission spectroscopy. The advantage of this method over conventional atmospheric transmission spectroscopy is that it does not rely on accurate photometric comparisons of observations on and off transit, but instead depends on the relative velocity shifts of individual stellar absorption lines within the same on-transit spectra. We used an archival VLT/UVES data set to apply this method to HD209458. The amplitude of the Rossiter effect is shown to be $1.7^{+1.1}_{-1.2}$ m/sec higher in the Sodium D lines than in the weighted average of all other absorption lines in the observed wavelength range, corresponding to an increment of 4.3±3% (1.4σ). The uncertainty in this measurement compares to a photometric accuracy of 5×10^{-4} for conventional atmospheric transmission spectroscopy, more than an order of magnitude higher than previous attempts using ground-based telescopes. Observations specifically designed for this method could increase the accuracy further by a factor $2-3$.

Key words: binaries: eclipsing - planetary systems - techniques: spectroscopic - stars: individual: HD209458

1 INTRODUCTION

Since the discovery that the extra-solar planet HD209458b transits its host star (Charbonneau et al. 2000; Henry et al. 2000; Mazeh et al. 2000), many attempts have been made to detect its atmosphere using transmission spectroscopy. During a transit, light that passes from the star through the outer parts of the planet's atmosphere has impressed on it a spectrographic signature of the atmospheric constituents, which can be observed as an extra absorption on top of the stellar spectrum (Seager & Sasselov 2000; Brown 2001; Hubbard et al. 2001). Observations with the Hubble Space Telescope (HST) using this technique have been a great success. First the Sodium D feature was discovered by Charbonneau et al. (2002) with a relative depth of 0.02%, followed by the detection of very strong absorption features at a $5-10$% level in the ultra-violet from Hydrogen, Oxygen and Carbon (Vidal-Madjar et al. 2003; 2004). The latter most likely come from the 'exosphere' of HD209458b, an extended cometary tail of gas evaporating from the planet caused by its migration close to the star (eg. Schneider et al. 1998).

In strong contrast, attempts to detect the atmosphere of HD209458b from the ground have so far been unsuccessful. So far, only upper limits of typically 1-2% have been reached, for the Sodium D feature in the optical (Brown et al. 2000; Bundy & Marcy 2000; Moutou et al. 2001), and for He, CO, H_2O and CH_4 in the near-infrared (Brown et al. 2002; Harrington et al. 2002; Moutou et al. 2003).

Ground-based observations suffer greatly from the fact that transmission spectroscopy relies on the comparison of spectra on and off transit, which are necessarily taken on different nights. This limits the accuracy due to varying weather conditions and instability of the instruments. In this paper a new method for probing the atmospheres of transiting exoplanets is presented, making use of the Rossiter effect. Due to the rotation of the host star, a transiting planet will first block off light from the approaching and then from the receding parts of the stellar surface. This results in an artificial wobble in radial velocity, an effect first observed by Rossiter (1924) for the eclipsing binary β Lyrae. The amplitude of this signal is di-

⋆ E-mail: ignas@roe.ac.uk

Table 1. The log of the observations, with in column 1 the date, in column 2 the total the exposure time, in column 3 the typical signal to noise ratio per exposure, in columns 4 and 5 the range in airmass and seeing, and in column 6 the orbital phase of HD209458b.

Data Set	Observing Date	Exposure Times (sec)	S/N	Airmass	Seeing ($''$)	Phase	Comments
1	05/08/2002	15×400	400	1.407−1.558	∼2	−0.007,+0.021	on transit
2	11/08/2002	15×400	535	2.151−1.394	0.9−1.5	+0.663,+0.693	off transit
3	12/08/2002	15×400	515	1.391−2.085	0.6−0.9	−0.012,+0.017	on transit
4	15/08/2002	15×400	475	1.388−1.704	0.7−1.7	+0.826,+0.857	off transit
5	13/09/2002	15×400	485	1.958−1.385	0.8−1.8	+0.003,+0.026	on transit
6	20/09/2002	15×400	515	1.695−1.384	0.7−1.0	−0.009,+0.020	on transit
7	22/09/2002	15×400	590	1.446−1.493	0.5−1.0	+0.569,+0.599	off transit

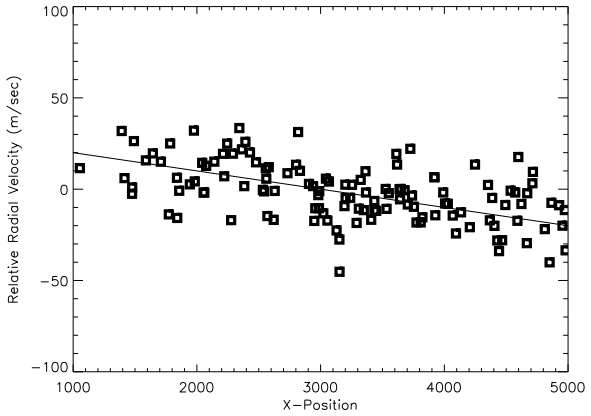

Figure 1. An example of the change in wavelength solution between two exposures. The x-position is the pixel position of a line within its order. The relative radial velocity indicates the change in velocity of a line between the two exposures, corrected for a global velocity shift. This effect is removed from the data by fitting the data points with a 3rd order Chebyshev function (solid line).

rectly proportional to the effective size of the transiting planet, and the wavelength dependence of this effect can reveal atmospheric absorption features, in the same way as with transmission spectroscopy. The advantage of this method is that it does not rely on accurate photometric comparison of spectra in and out of transit, but instead depends on relative velocity shifts of stellar absorption lines in the same in-transit spectra.

2 OBSERVATIONS, DATA REDUCTION, AND ANALYSIS

We applied this new method to an archival data set of HD209458 taken with the UV-Visual Echelle Spectrograph (UVES) on the Very Large Telescope. This data was originally obtained to perform conventional atmospheric transmission spectroscopy (PI: Moutou et al., project 69.C-0263). Data was collected during 7 nights (4 on, and 3 off transit) through UVES' red arm only, using the CD3 cross disperser with a blaze wavelength of 5600 Å, and image slicer nr. 3, consisting of 5 slices of 0.3" width each. Each night a series of 15 data frames were taken with exposure times of 400 sec. A calibrator was observed after the 5th and 10th frame each time, leaving gaps of ∼25 min. The observation log is given in table 1.

The detector in the red arm of UVES consists of a mosaic of two 4k×2k CCDs. For our analysis we concentrated on one CCD, covering a wavelength range of 5850 to 6550 Å over 16 echelle orders, and which contains the two Sodium D lines (5890.0 & 5895.9 Å) in its first order. The data reduction was performed in a standard manner, using ESO's UVES data reduction pipeline, which is part of the software package MIDAS. Data from each echelle order was kept separately, with the output data of each frame consisting of a 2 dimensional array with wavelength position along the x-axis (pixel size = 0.0174 Å), and echelle order along the y-axis. The resolving power was typically ∼110,000. The orbital phase of HD209458b was determined for each observation using the orbital parameters as derived by Brown et al. (2001), and were corrected for variations in light traveling time through the solar system. A global phase-shift of 0.008 (40 min.) had to be applied to all data sets to centre the Rossiter effect at zero phase. This shift corresponds to an error in the period derived by Brown et al. of 8 sec.

The subsequent data analysis on the 2 dimensional data frames was performed in IDL. First the spectrum in each order was fitted with a 7th order Chebyshev function away from absorption features, and normalised. Further analysis consisted of the four steps described below. Since some of their input and/or output are inter-dependent they are performed several times before the final results were produced.

Step 1: Absolute wavelength calibration. The absolute wavelength calibration was determined from the wavelength positions of the strong H_2O telluric lines between 6275Å and 6320Å (in the 4th echelle order). First a model of the stellar absorption spectrum of HD209458 was produced from the velocity shifted and median filtered spectra obtained during the 7 nights. This model was then appropriately shifted and subtracted from each frame, leaving only the telluric line absorption. The dozen strongest lines were fitted with Gaussians and their positions compared with the spectral atlas of telluric line absorption of Pierce & Breckenridge (1974). After several iterations, necessary to obtain the best stellar model, the absolute wavelength calibration is found to be accurate to ∼5-10 m/sec.

Step 2: Fitting of the stellar absorption lines. The wavelength positions of the ∼300 strongest absorption lines were determined by least-square fitting of an area of 40 pixels centred around the minimum of each absorption line. The accuracy of this method was estimated by measuring the standard deviation around the mean position of the line during each night, corrected for earth rotation and orbital motion and changes in the wavelength solution. The two Sodium D lines were fitted in a similar way, but with a 4 parameter Moffat function instead of a Gaussian.

Step 3: Relative wavelength calibration. It was found that the relative positions of the strong emission lines varied much more than expected, and that these variations were a function of the position of a line within its order (a typical example is shown in Figure 1). A similar but generally smaller trend was also found as func-

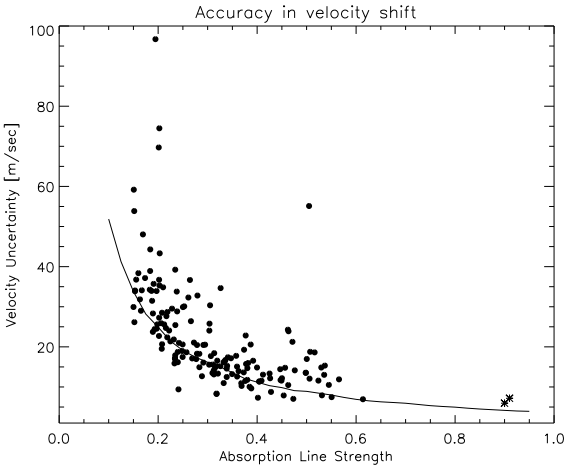

Figure 2. The accuracy in radial velocity as function of the absorption line strength for one of the data sets. This is estimated from the scatter around the mean position of each line. The two Sodium D lines are indicated by stars. The solid line indicates the expected uncertainty due to Poisson noise for a spectrum with a signal-to-noise ratio of 500 per spectral element. An accuracy of 5−10 m/sec is reached for the strongest lines.

tion of the echelle order. These effects are most likely caused by small changes in the instrument settings and/or temperature of the spectrograph from exposure to exposure. We simply corrected for these trends by fitting relative positions of the ∼100 strongest lines as function of their pixel position with a 3rd order Chebyshev function, and with a 2nd order polynomial as function of the echelle order. The residual scatter around the best fits are found to be typically 10−15 m/sec. This correction in the wavelength solution is applied to all lines.

Step 4: Removal of telluric line emission. Great care has to be taken in the removal of telluric line absorption, especially around the Sodium D line at 5889.9 Å. A small change in the strength of the telluric absorption can introduce a significant shift in radial velocity, if it is located within the fitting region of the stellar absorption line. Using the best wavelength solution available, a model of the stellar spectrum of HD209458, as obtained above, is subtracted from the data, leaving only the telluric lines. Using the line list of Pierce & Breckenridge (1974), the telluric absorption lines are fitted with Gaussians, with the amplitude as only free parameter, and are subsequently removed.

The accuracy in radial velocity achieved for one of the data sets is shown as function of the absorption line depth in Figure 2. It shows that for the strongest lines, such as the Sodium D lines, an accuracy of 5-10 m/sec has been reached. Monte-Carlo simulation were performed to determine the theoretical uncertainty as function of absorption line strength, assuming a signal to noise ratio of 500 per spectral element. This is indicated by the solid line.

3 RESULTS

First the overall strength of the Rossiter effect of HD209458 was determined. The weighted mean of the radial velocities of all absorption lines was determined for each exposure, and subsequently corrected for the star's motion induced by the exoplanet (assuming an amplitude of 85.9 m/sec; Mazeh et al. 2000), the motion and rotation of the Earth, and for the shifts in the absolute wavelength calibration as determined above. The same corrections were applied to the radial velocities of the two sodium D lines. The 4 on-transit data sets were then merged by applying small global $0-5$ m/sec offsets to the data to minimise the scatter in the combined velocity curve. The merged velocity curves are shown in figure 3, which are fitted to models of the Rossiter effect. Our models are constructed in a similar way as in Queloz et al. (2000), by simulating the transit of a dark object over a limb-darkened star. A spherical star with uniform rotation is considered, with the orbital motion of the planet and the stellar rotation set in the same direction. The angle between the orbital plane and the equatorial plane is assumed to be zero, and the impact parameter is set to 0.5, corresponding to the orbital inclination of 86.6° as determined by Brown et al. (2001). The star is divided into 200,000 cells, with the spectrum of each cell modeled by a Gaussian absorption line with $\sigma = 4.0$ km/sec. The overall integrated spectrum is made by summation of the cells free of the planet along the line of sight.

The aim of this modeling is to set the amplitude scale of the Rossiter effect relative to the depth of the photometric transit. Limb darkening is assumed to be of the form $B_\mu = 1 - \epsilon(1-\mu)$, where μ is the cosine of the angle between the line of sight and the normal to the local stellar surface, and ϵ is assumed to be 0.58 (Deeg et al. 2001). The influence of wavelength dependent limb-darkening is discussed below. Assuming a ratio of planet to star radius of 0.118 (Brown et al. 2001), the overall velocity curve is best fitted with a stellar $v\ sin\ i$ of 4.5 km/sec, resulting in an amplitude of the Rossiter effect of about 38 m/sec (see figure 3). This amplitude corresponds to the photometric transit depth of 1.6% (Brown et al. 2001), meaning that an excess of 1 m/sec compares to a signal for conventional atmospheric transmission spectroscopy of 0.04%.

The excess of the Rossiter effect in the Sodium D lines

The mean radial velocity of each exposure were then subtracted from that of the Sodium D lines to reveal any possible excess in the Rossiter effect. The global velocity shifts applied above cancel out, but new global velocity shifts were applied to each data set, to set the mean relative velocity shift of all 15 exposures to zero. Ideally, the observations should have cover a substantial period before and after the transit to set the zero-point independently from the in-transit data (see below). The velocity shifts of the Sodium D lines compared to the average of all other lines is shown in figure 4. The scatter in the four data sets is 6.5, 3.7, 7.6, and 4.7 m/sec respectively. The right panel shows the data binned together, using time-bins of 450 seconds. The dispersion around zero in this binned data set is 4.7 m/sec. The data set is fitted with the model described above, with all parameters fixed except the amplitude of the signal. The best fit gives an amplitude of $1.7^{+1.1}_{-1.2}$ m/sec, corresponding to a photometric signal using conventional atmospheric transmission spectroscopy of $7\pm5\times10^{-4}$.

4 DISCUSSION AND CONCLUSIONS

The analysis of the UVES archive data shows that the Rossiter effect provides a powerful tool to probe the atmospheres of transiting exoplanets. Although no significant signal has been detected for Sodium D in HD209458b, it is the first time that ground-based observations result in an accuracy of $<$0.001. Previous ground-based observations have reached accuracies of only 1−2%, corresponding to an excess in the Rossiter effect of 20−50 m/sec, clearly inferior to the precision achieved here.

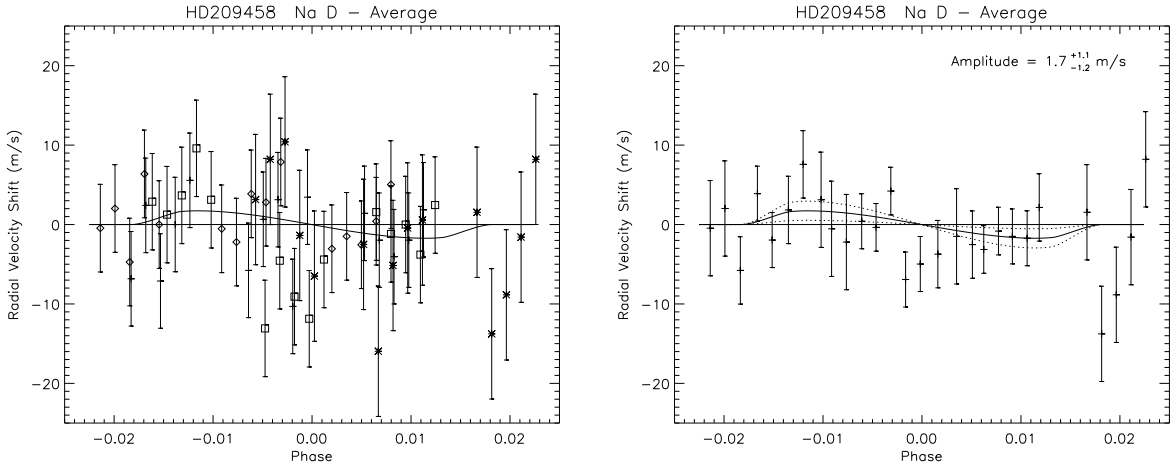

Figure 4. The excess of the Rossiter effect in Sodium D, using the individual data points (left panel) and binned data (right panel). The best fit gives an amplitude of $1.7^{+1.1}_{-1.2}$ m/sec, and is shown by the solid line. The 1σ confidence limits are indicated by the dotted lines. This corresponds to a photometric signal using conventional transmission spectroscopy of $7\pm5\times10^{-4}$. The symbols are as in figure 3.

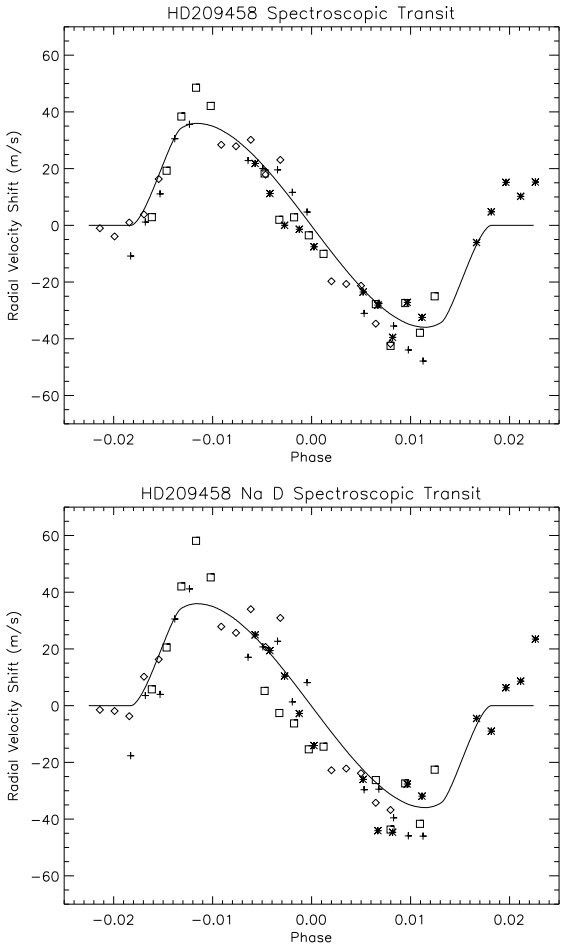

Figure 3. The Rossiter effect as observed for HD209458, using the weighted average of the ∼100 strongest absorption lines (upper panel), and the average of the two Sodium D lines (lower panel). Data from the four on-transit data sets are indicated with boxes - set 1, diamonds - set 2, stars - set 4, and crosses - set 5. Our best model is indicates by the solid line.

The HST Transmission spectrum of HD209458b obtained by Charbonneau et al. (2002) revealed an excess in absorption in Sodium D of 0.00023 compared to the surrounding continuum, implying a relative increase of ∼1.8%. This indicates that for this particular absorption feature an excess in the Rossiter effect of ∼0.7 m/sec can be expected, making its detection very challenging for the current instrumentation. However, it is important to realise that the excess in absorption as determined with the HST was measured over a bandwidth of 12Å. In contrast, line-to-line variations in the Rossiter effect will be most sensitive to planetary absorption on scales of the half-power width of the stellar lines (a fraction of an Ångstrom). Most models of transmission spectra (eg. Brown 2001) indicate that on this scale the absorption signal for Sodium D could be $2-5$ times higher ($1-3$ m/sec).

The archival data sets used in this paper are not optimal for measuring the Rossiter effect. First of all, since a significant fraction of the time was devoted to calibrators, typically only 60% of the on-transit time was spent on target, and on several occasions the periods that the amplitude of the Rossiter effect is expected to be the strongest were missed. In addition, the current analysis is significantly hampered by the fact that no or hardly any time was spent on target directly before or after each transit. This was often dictated by the timing of the transit and visibility of HD209458 from Paranal. For the most optimal transits, HD209458 can be observed from 1 hour before to 1 hour after the overall transit with the VLT. In those cases the zero-point in velocity can be determined independently from the on-transit data, and one could also correct for any possible residual drifts in radial velocity over the transit, eg. due to residual telluric absorption line features or inaccuracies in flat fielding. Overall, this should result in an increase in precision of a factor $2-3$. It means that, if the current value is believed, a $3-5$ σ detection of Sodium D should be possible over a couple of transits.

Wavelength variations in limb-darkening

The exact shape and amplitude of the Rossiter effect are dependent on the stellar limb darkening. So far we have not taken into account that limb darkening decreases as function of wavelength. Furthermore, the limb darkening effect also changes differently over the

profile of each absorption line. Here we assess the possible influence of both effects. The wavelength dependence of the limb darkening of HD209458 has been observed by Deeg et al. (2001), with ϵ changing from 0.62 at 5900 Å to 0.58 at 6180 Å. To estimate the influence of this effect we assumed a linear wavelength dependence of $\epsilon(\lambda) = 1.46 - \lambda/7000\AA$, and calculated the change in radial velocity for each line relative to that of Sodium using the model described above. By incorporating this wavelength dependent limb-darkening, the excess of the Rossiter effect in the Sodium D lines is increased by $\sim$0.2 m/sec.

The variations in limb darkening across solar absorption lines is studied in great detail by Pierce & Slaughter (1982) for Sodium D, and by Balthasar (1988) for a whole range of bright absorption lines, by measuring changes in the absorption line depths across the solar disk. The strength of this effect is dependent on the mechanism of formation of the line. Most absorption lines weaken towards the limb of the Sun, meaning that the limb darkening in the centre of the lines is less than in the surrounding continuum. Assuming that this effect is similar for HD209458 as for the Sun, our modeling indicates that these variation contribute at a level of again $\sim$0.2 cm/sec. Although this is insignificant for these data, it means that future observation aimed at measuring variations in the Rossiter effect at much higher precision should take these effects into account.

Future applications for this method

We believe that the new method presented here to probe atmospheres of transiting exoplanets using the Rossiter effect, has great potential. Specifically targeted observations, rather than the archival data used here, can increase the accuracy further by a factor $2-3$. Furthermore, in the near-infrared, where the atmospheric absorption features due to H_2O, CO, and CH_4 cover many stellar lines, a great improvement over current observations can be reached. Although confusion with water-vapor and methane in the earth atmosphere will complicate the analysis. In addition, anticipating the discovery of exoplanets transiting bright stars of either later spectral type (with many more stellar lines to average), or with faster stellar rotations (resulting in a Rossiter effect with a higher amplitude), a further significant increase in accuracy can be expected.

ACKNOWLEDGEMENTS

I would like to thank Philip Best for useful discussions and for carefully reading the manuscript. This research is based on observations made with the European Southern Observatory telescopes obtained from the ESO/ST-ECF Science Archive Facility.

REFERENCES

Balthasar H., 1988, A&AS 72, 473
Brown T.M., Butler R.P., Charbonneau D., Noyes R.W., Sasselov D., Libbrecht K.G., Marcy G.W., Seager S., Vogt S.S., 2000, 197th AAS Meeting, 11.05; BAAS, Vol. 32, p.1417
Brown T.M., 2001, ApJ 553, 1006
Brown T.M., Charbonneau D., Gilligand R.L., Noyes R.W., Burrows A., 2001, ApJ 552, 699
Brown T.M., Libbrecht K.G., Charbonneau D., 2002, PASP 114, 826
Bundy K.A., Marcy G.W., 2000, PASP 112, 1421
Charbonneau D., Brown T.M., Latham D.W., Mayor M., 2000, ApJ 529, 45
Charbonneau D., Brown T.M., Noyes R.W., Gilligand R.L., 2002, ApJ 568, 377
Deeg H.J., Garrido R., Claret A., 2001, NewA, 6, 51
Harrington J., Deming D., Matthews K., Richardson L.J., Rojo P., Steyert D., Wiedemann G., Zeehandelaar D., 2002, 201st AAS Meeting, 46.04; BAAS, Vol. 34
Henry G.W., Marcy G.W., Butler R.P., Vogt S.S., 2000, ApJ 529, L41
Hubbard W.B., Fortney J.J., Lunine J.I., Burrows A., Sudarsky D., Pinto P., 2001, ApJ 560, 413
Mazeh T., Naef D., Torres G., Latham D.W., Mayor M., Beuzit J.-L., Brown T., Buchlave L., Burnet M., Carney B.W. et al. 2000, ApJ 532, L55
Moutou C., Coustenis A., Schneider J., St Gilles R., Mayor M., Queloz D., Kaufer A., 2001, A&A 371, 260
Moutou C., Coustenis A., Schneider J., Queloz D., Mayor M. 2003, A&A 405, 341
Pierce A.K., Breckenridge J.B., Kitt Peak National Observatory Contribution, Tucson: Kitt Peak National Observatory, 1974
Pierce A.K., Slaughter C., 1982, ApJS 48, 73
Queloz D., Eggenberger A., Mayor M., Perrier C., Beuzit J.L, Naef D., Sivan J.P., Udry S., 2000, A&A 359, L17
Rossiter R.A., 1924, AJ 60, 15
Seager S., Sasselov D.D., 2000, ApJ 537, 916
Schneider J., Rauer H., Lasota J.P., Bonazzola S., Chassefiere E., 1998, in "Brown dwarfs and extrasolar planets", eds R. Rebolo, E.L. Martin; M.R. Zapatero Osorio, ASP Conference Series 134, 241
Vidal-Madjar A, Lecavelier des Etangs A., Désert J.-M., Ballester G.E., Ferlet R., Hébrard G., Mayor M., Nature 422, 143
Vidal-Madjar A, Désert J.-M., Lecavelier des Etangs A., Hébrard G., Ballester G.E., Ehrenreich D., Ferlet R., McConnell J.C., Mayor M., Parkinson C.D., 2004, ApJL submitted